International Journal of Pharmacology

ISSN 1811-7775

science alert

ansinet
Asian Network for Scientific Information

OPEN ACCESS International Journal of Pharmacology

ISSN 1811-7775
DOI: 10.3923/ijp.2021.621.633

Research Article
Nanosize Hydroxyapatite Significantly Repairs the Bone Damage Caused by Several Genes

[1]Yang Liu, [1]Hao Liu and [2]Chengli Liu

[1]Department of Traumatic Orthopedics, Cangzhou Hospital of Integrated Traditional Chinese and Western Medicine of Hebei Province, Cangzhou, 061000, China
[2]Reproductive Medicine, Cangzhou Hospital of Integrated Traditional Chinese and Western Medicine of Hebei Province, Cangzhou, 061000, China

Abstract

Background and Objective: Hydroxyapatite (HA) is a naturally occurring mineral type of calcium apatite, calcium, phosphorus and oxygen. Which makes up most of the bone structure of humans, forms tooth enamel and presents in small amounts in the brain. The purpose of this study was to synthesize nano-sized hydroxyapatite particles as a synthetic medicine for the gene mutations which cause bone damage. **Materials and Methods:** For this purpose, an aqueous solution of calcium nitrate tetrahydrate and diammonium hydrogen phosphate at pH 10 was used. Furthermore, molecular docking was performed to determine the interactions of HA with several mutated genes (BMP2, COL1A, IGF-1, PDGF and TGF-β) which are responsible for bone damage to determine its efficacy as a therapy against these mutated genes. **Results:** HA size was ranging from 100-200 nm, after synthesis, HA did not decompose into any other step, even after 1 hr of air heating at 1000°C, which confirmed its stability. In all the docked complexes, lower binding energies (-7.088 to -11.673 kcal mol^{-1}) and positive binding efficiencies, 0.79-0.89 kcal mol^{-1} were obtained which validated molecular docking results. Both the synthesis and the molecular docking results indicated that HA is a better binding agent to correct bone damage and can be used as a bone implant. **Conclusion:** HA is a potent inhibitor of mutated bone healing genes (BMP2, COL1A, IGF-1, PDGF and TGF-β). In the future, this work can be further accessed in clinical trials to determine the efficacy of HA against the above-listed gene mutations.

Key words: Bone damage, co-precipitation, hydroxyapatite, tissue repair, gene mutations

Citation: Liu, Y., H. Liu and C. Liu, 2021. Nanosize hydroxyapatite significantly repairs the bone damage caused by several genes. Int. J. Pharmacol., 17: 621-633.

Corresponding Author: Chengli Liu, Reproductive Medicine, Cangzhou Hospital of Integrated Traditional Chinese and Western Medicine of Hebei Province, Cangzhou, 061000, China

Competing Interest: The authors have declared that no competing interest exists.

Data Availability: All relevant data are within the paper and its supporting information files.

INTRODUCTION

Bone loss and subsequent recovery are the key problems of orthopaedics and their related clinicians. Good knowledge of the principles underlying bone degradation and recovery is crucial to the management of serious fractures, including bone deficiency, osteonecrosis, arthritis, spinal fusion, osteoporosis, osteolysis-related wear of particles, chronic bone disease, cancer and other bone-affected diseases. Bone loss and reconstruction is a problem of great economic significance. Bone fractures due to fragility are a second major cause of pain and disability affecting women (50%) and men (25%) over 50 years of age[1,2]. Bone is a highly complicated tissue that undergoes a comprehensive recovery procedure to cope with the increased mechanical stress and repairing fractures that induce fatigue[3].

In addition to this type of remodelling, bone has immense potential for regeneration. Bone can heal fully under ideal conditions without developing a fibrous scar in a manner that is indistinguishable from injury. The healing mechanism for fractures is particularly complex and it is challenging to understand in certain respects[4]. However, certain universal principles that direct bone regeneration has been well established with major factors that greatly affect the outcome of healing. About 10-15% of all fractures heal with prolonged immobilization and delayed recurrence[5]. Still, the pathomechanism of damaged skeletal tissue repair continues undistinguished following exceptional tests. Clinical and laboratory work has an established understanding of growth factors (molecular regulators), cytokines and chemokines that regulate cellular events that occur in fracture gaps[6]. It also revealed a pronounced decline or lack of essential molecular expression[7].

Other essential molecular factors for wound healing have been reported in Genetic research, including bone morphogenetic protein 2 (BMP-2), collagen type 1 (COL1A), a molecular protein that regulates healing factors; insulin-like growth factor (IGF-1), platelet-derived growth factor (PDGF) and transforming growth factor (TGF-β)[8]. Collagen is an essential natural constituent of the extracellular bone network, abundant in nature which provides strength and flexibility to bone[9]. More specifically, BMP1 and BMP2 are primarily involved in the production assembly and function of collagen 1; defects in one of the genes responsible for the COL1A synthesis ultimately cause fracture and brittle bone disease having low bone density[10].

Defects in the TGF-β gene cause an unusual monogenic disorder of enlarged bone mass due to rapid bone development. Both *in vivo* and *in vivo* studies have shown that the TGF-β signalling pathway can influence the development and resorption of bone and is an effective controller of bone remodeling[11]. IGF-1 plays an important role in stimulating the production of growth hormone, which is produced in every cell of the body, including the bones. IGF-1 seems essential during growth and adult bone mass preservation for longitudinal bone development, skeletal maturation and bone mass securing. Outbreak or inhibition of IGF-1 results in osteoporosis-related fractures that create a significant health issue[12]. PDGF works as an excellent bone fixer and rebuilder, it also contributes to the osteogenic tradition and helps strengthen newly developed vessels to facilitate multi-stage, multi-component production of new bones[13].

Therapies for bone fracture injury include repairing and stabilizing the wound or bone grafting and applying osteoid tissue to the affected place. In addition to those treatments, pharmaceuticals have been used to assist the regeneration of the bone tissue, such as the use of bisphosphonates, BMP7[14]. Some bone materials have also been developed and provided excellent guarantees for bone healing, like nano-products, strengthened bone cell functions relative to their micron-sized partners and other feasible types of bone fracture fixing products[15]. The nanomaterials are organic or natural materials, the thickness of which is less than 100 nm. Any nano-sized substance can technically be treated as a nanomaterial but the scale for better applications in biomedicine should be between 10-100 nm[16].

$Ca_{10}(PO_4)_6(OH)_2$ (hydroxyapatite, HA) is the basic mineral composition of bones and teeth[17], Due to its compatibility, activity and very low solubility in wet media, $Ca_{10}(PO_4)_6(OH)_2$ (hydroxyapatite, HA) is emphasized in orthopaedic surgery and orthopaedic surgery[18]. Henceforth nano-HA powder engineered as a bone repair and the strengthening agent is of considerable importance in biomedical composites. These nanoceramics have been used to support the production of new bones for osteographic coatings on metal inserts[19]. Several methods have been discussed for HA synthesis, including solid-state synthesis[20], sol-gel techniques[21], spray pyrolysis[22], solvothermal processes[23] and chemical vapour deposition[24]. The objective of this research was therefore the synthesis of nano-sized HA as a treatment measure for the reconstruction of bone damage induced by mutations in the BM2, COL1A, IGF-1, PDGF and TGF-β genes and its interactions analysis with these genes using molecular docking.

MATERIALS AND METHODS

Study area: The experimental study was carried out in the Traumatic Orthopedics Department, Cangzhou Hospital of Integrated Traditional Chinese and Western Medicine of Hebei Province (CZITCW202009X), China from May, 2020 to Feb, 2021.

***In vivo* synthesis of hydroxyapatite for bone repair:** Two precipitation methods for the HA synthesis have been reported in the literature[25-27]. The first process requires combining 0.6 m phosphoric acid solution with a 1 m calcium hydroxide solution:

$$10\left[Ca\,(OH)_2\right]+6H_3\,PO_4 \rightarrow \left[Ca_{10}(PO_4)_6(OH_2)\right]+18\,H_2O$$

The second co-precipitation process focused on applying diammonium hydrogen phosphate to calcium nitrate and ammonium solution as a pH adjuster:

$$6\left[((NH_4)_2\,HPO_4\right]+10\left[\left(Ca(NO_3).4H_2O\right)\right]+$$
$$8NH_4OH \rightarrow 20NH_4NO_3+\left[Ca_{10}(PO_4)_6(OH)_2\right]+46H_2O$$

Reagents: The 98% Diammonium hydrogen phosphate ($(NH_4)_2HPO_4$), 98% Calcium hydroxide ($Ca(OH)_2$), 99% Calcium nitrate Tetrahydrate ($Ca(NO_3).\,4H_2O$), 97% Phosphoric acid (H_3PO_4), 28% aqueous solution of Ammonium hydroxide solution ($NH_4OH_{(aq)}$), poly (vinyl alcohol) 2.5 g, 500 mL distilled water and deionized water were used throughout the experiment.

Experimental

Synthesis of nanometer hydroxyapatite powder materials: Nano-sized HA was synthesized utilizing a co-precipitation technique (2nd method), 0.25 m solution of Calcium nitrate and 0.15 m Diammonium hydrogen phosphate solutions were used. The pH was set to 10 while adding 5 mL Ammonium hydroxide solution to the Calcium nitrate solution and 10 mL of Ammonium hydroxide to the Diammonium hydrogen phosphate solution collectively through continuous mixing. About 250 mL ionic solutions of PO_4^{3-} was poured into 250 mL ionic solution of Ca^{2+} dropwise with a flow rate of 10 mL min^{-1} to yield an amorphous precipitate of Hydroxyapatite at 50°C. During the inclusion of solutions, the suspension pH was continuously monitored, reactions that occurred in basic conditions contributed to the development of HA. The aqueous suspension was stored for 15 hrs and later distributed in 45 mL de-ionized water, supplemented by a vortex blender, three washing cycles were performed respectively to get HA powder. The wet residues were then oven-dried at 90°C for 12 hrs until further analysis. HA sand was obtained after drying.

Preparation of porous and dense samples: The 50 g of the collected HA powder was combined with 2.5 g of poly (vinyl alcohol) and 100 mL purified water for the preparation of dense samples. Suspension homogenization was done using a magnetic stirrer by spray drying. The well-dispersed powder obtained was then compressed with a cold-pressing method of 800 kg cm^{-2} and the HA granulates obtained were sintered in the air for 1 hr at 1250°C. The 25% of the HA powder was primed as a dispersant to prepare the slurries for the porous sample preparation. Commercial cellulose sponges were tested and the initial impregnation process was used with considerable slurry fluidity. To extract organic matter the sponges were then dried in the slurry in fresh air for 72 hrs and then heated for 1 hr at 600°C. Sintering was carried out at 1250°C for 1 hr.

The mass of porous and dense bodies was calculated as apparent density (geometrical weight/volume measurement). The compressive pressure was measured using an Instron 1195 apparatus on cylindrical specimens (10 mm height × 10 mm diameter). The compressive strength was determined from the full load, divided by the original area, recorded during the test. For this study, multiple specimens were used. Nano rods of 25×2.0×2.5 mm polycrystalline hydroxyapatite were extracted from cylindrical plates with a diamond saw. Until inspection, no further chemical treatment was done on the rods. Flexural experiments were done using a Lloyd LR10 K plus mechanical tester in four-point bending.

***In silico* studies of hydroxyapatite:** The 3D structure of Hydroxyapatite was designed in Chemdraw software and saved in mol2 format. The chemical composition of HA was tested for various mechanisms of toxicity including hepato-toxicity, immune-toxicity, cytotoxicity, mutagenicity and carcinogenicity using the Protox II server. Knowledge of the genes responsible for bone healing was obtained by literature[10-13] and their 3D mutated structures were selected because of their inability to repair bone damage. The 3D structure of BMP2 protein, COL1A protein, IGF-1, PDGF protein structure and TGF-β were downloaded from the Protein Database (PDB)[28]. The 3D structures of proteins and the 3D structure of HA ligand are shown in Fig. 1(a-f). Mutated protein binding pockets were identified through Pock Drug; a pocket item prediction server[29].

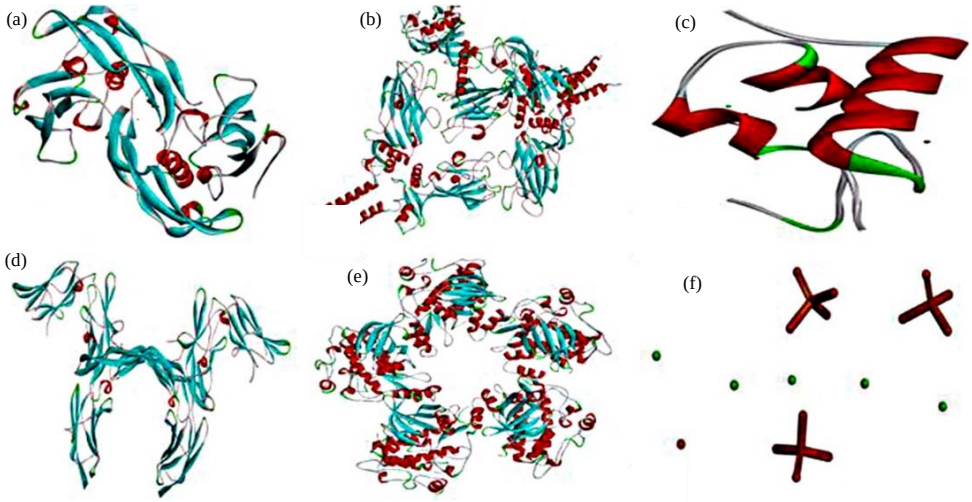

Fig. 1(a-f): 3-dimensional structures of the proteins and HA ligand, (a) BMP2 protein, (b) COL1A protein, (c) IGF-1 protein, (d) PDGF protein, (e) TGF-β protein and (f) Hydroxyapatite ligand

Both ligand and protein structures were prepared for docking and imported to Auto dock Vina. Water molecules were removed from the protein structures, hydrogen atoms were added, charges were allocated to the atoms using the force-field method. All the Protein structures were prepared using the standard procedure. Minimization of the protein structure was done until the average Root Mean Square Deviation (RMSD) of non-hydrogen atoms attained less than 1 Å. Based on drug score and standard deviation score, the torsions were added to the ligand and molecular charge was assigned, then the HA ligand was docked into the mutated pockets of all proteins one by one. The RMSD value was set at 2 Å for each docked complex. The docking results with higher score values were selected based on score ranking and analyzed in the discovery studio software for interactions among ligand and receptors to confirm the use of HA against these mutated genes as a repairing agent to overcome bone damage.

To test stability and further confirm the docking findings, the docking studies were forwarded to Molecular Dynamics (MD) simulations using the GROMACS instrument. A simulation run was performed for 10000 ns using the CHARMM force field and a dodecahedral box was subsequently created and neutralized with counter ions for each 1 nm thick protein water model. Using the steepest descent algorithm to expel poor connections, the scheme was reduced by 1,000 steps. The balancing method was then carried out by constant number, volume and temperature (NVT) and constant number, pressure and temperature (NPT) refraining the backbone of the protein and allowing stability of the solvent molecules and counter ions. The NVT was conducted at 300 K for 1 ns with a V-rescale thermostat used to maintain steady temperatures. Using Parrinello-Rahman barostat, the NPT was done for 1 ns at 1 bar. The bonds of heavy atoms were removed and the Particle Mesh Ewald (PME) system was used to calculate long-range electrostatic interactions. The short-range connections were estimated using a 12 Å cut-off point. With a time stage of 2 ns, the MD was done under periodic boundary conditions to avoid edge effects, saving the coordinate data for every 1 sec. The results were analyzed in Discovery Studio.

RESULTS

A concentrated solution was produced as soon as the reaction mixture was refluxed at 100°C for 4 hrs. This was gradually converted into a white gel by evaporation of the in-situ solvent. The reaction of the Hydroxyapatite production may be expressed as follows:

$$5Ca(NO_3)_2 + 3(NH_4)_2HPO_4 + 4NH_4OH \rightarrow Ca_5(PO_4)_3OH + 10NH_4NO_3 + 3H_2O$$

The obtained black dried gel was then subjected to TG-DTA. The first weight showed the gel dried DTA-TG at 350°C. Water evaporation falls to 10% at 100°C. A subsequent weight reduction occurred at 700°C, 50% due to the decomposition of ammonia, nitrate, urea, chemical contaminants and carbon dioxide. The Hydroxyapatite powder was produced under moving dust by the calcinations of dry gel at 820°C for 2 hrs, this yielded 90-95% pure HA powder. The collected HA powder was then subjected to transmission electron microscope (TEM) analysis, which

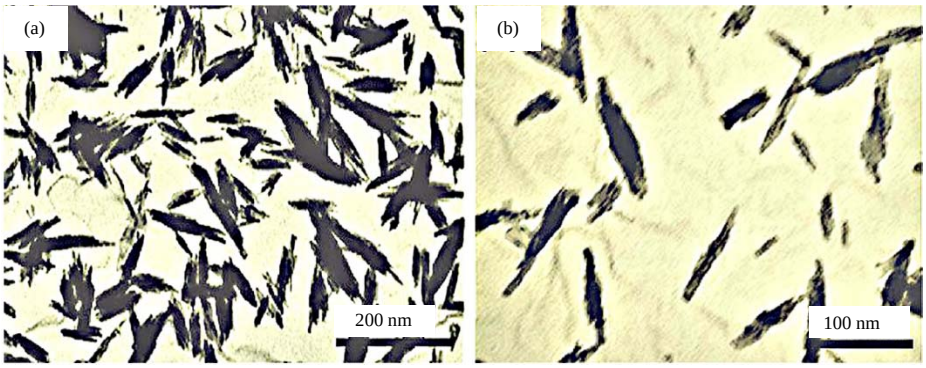

Fig. 2(a-b):TEM images of hydroxyapatite nano-rods, prepared using co-precipitation method based on calcium nitrate and diammonium precursors of hydrogen phosphate, (a) 200 and (b)100 nm sized HA bars

Table 1: Physical properties of the dense and porous nano-size HA powder

Type of HA powder	Sintering temperature (°C)	Flexural strength (MPa)	Density (g cm^{-3})	Relative density (%)
Dense bodies	1250	56.9	2.346	91
Porous bodies	1250	1.89	1.180	63

verified the existence of tiny crystallites. Pure Hydroxyapatite nanoparticles were synthesized by co-precipitation have shown a rod-like structure, with an average length roughly equal to ~113±10 and ~13±10 nm (250 particles) along the smaller axis in Fig. 2a and b. Figure 2a and b show small crystallites have developed. The phase-pure HA nanoparticles produced had a rod-like morphology, with an average length of ~113±10 (250 nm particles) along the longest axis and ~13±10 (100 nm particles) along the smaller axis. Images were collected for both prepared and heat-treated nano-HA samples at 1000°C for 1 hr.

The probability of calcium hydroxide present in the powder was also tested. A phenolphthalein examination confirmed that there was no hydroxide in the powder. The nanometric primary particles were strongly agglomerated into micrometric aggregates of varying shapes and sizes of rods like structures. On the other hand, two separate size distributions were shown by the particle size distribution of the hydroxyapatite powder as measured by the nanoparticle sizer; the lower distribution ranges from approx 50-500 nm may be attributed to individual particles and tightly bonded particle agglomerates may be attributed to the higher distribution from 2000-7000 nm. To assess the efficiency of the obtained HA powder, dense and porous bodies were prepared. For the HA powder, the sintered thick bodies displayed flexural strength of 56.9 MPa and an apparent density of 2.346 g cm^{-3} and a relative density of 91% (i.e., 10% porosity). Although the flexural intensity was not too strong, the flexural strength of human cortical bones is also in the range. As shown by the much higher mechanical capabilities of the present HA thick bodies, the sintering process at lower temperatures was adequate to achieve a comparable degree of particle densification.

The polymeric sponge method was also used to produce the subsequent macrostructure of the porous hydroxyapatite. The sample had open-cell circular pores in rod-like structures with a diameter of 500 microns-2 mm. The pore configurations were probably identical to those of the original matrix. After 1250°C sintering, a 41% sintering shrinkage was obtained, with an apparent density of 1.180 g cm^{-3} and a 63% relative density. On the other side, the compressive strength of 1.89 MPa was given by the calculation of the physical properties of porous bodies. The physical properties of both dense and porous HA nanoparticles are shown in Table 1.

The preliminary powder consistency test (Table 1) indicates that HA powders have outstanding physical properties that can be used to create the desirable properties of thick and porous bioactive bone implants. Table 1 showed the higher sintering temperature of 1250°C for both the dense and porous HA particles and the relative density of 91% for dense and 63% for porous HA particles, confirming its appropriate synthesis. The synthesized HA ligand was then tested for the values of toxicity, LD50 and potential properties of absorption, distribution, metabolism and elimination (ADME) using Bioinformatics tools shown in Table 2 and 3.

It is verified from the probability values in Table 2 that all the values are less than 1.0, meaning that the synthesized nano-sized HA powder is non-toxic and would not cause any side effects. From Table 3 it is observed that the HA powder is non-toxic as it doesn't produce any type of toxic effects, it can

Table 2: Toxicity of synthesized nanosized hydroxyapatite predicted through the protox II server and PKCSM server to know its possible effects and maximum tolerated dose

Target	Prediction	Probability
Hepatotoxicity	NA	0.99
Carcinogenicity	NA	0.88
Immunotoxicity	NA	0.99
Mutagenicity	NA	0.74
Cytotoxicity	NA	0.78
AMES toxicity	NA	0.91
Maximum tolerable dose for human	Small	0.451
Human epidermal receptor growth factor I inhibitor	NA	0.55
Human epidermal receptor growth factor II inhibitor	NA	0.55
Oral acute toxicity in LD_{50} for rat	NA	2.118
Oral chronic toxicity for rat	Active	1.089
Sensitivity for skin	NA	0.89
T. piriformis toxicity	Active	0.286
Minnow toxicity	Active	0.527

Table 3: Pharmacokinetic properties of synthesized nano-HA in the form of its absorption, distribution, metabolism and elimination

Property	Model name	Predicted value	Unit
Absorption	Solubility of water	-3.908	Log mol L^{-1}
Absorption	Caco2-permeability	0.073	Log Papp in 10-6 cm s^{-1}
Absorption	Human intestinal absorption	0	Absorbed (%)
Absorption	Permeability for skin	-2.735	Log Kp
Absorption	P-glycoprotein substrate	Yes	Yes or No
Absorption	P-glycoprotein I inhibitor	No	Yes or No
Absorption	P-glycoprotein II inhibitor	No	Yes or No
Distribution	Human VDss	-1.316	Log L kg^{-1}
Distribution	Human unbound fraction	0.675	Fu
Distribution	Blood-brain barrier permeability	-3.026	Log BB
Distribution	Central nervous system permeability	-3.824	Log PS
Metabolism	CYP2D6 substrate	No	Yes or No
Metabolism	CYP3A4 substrate	Yes	Yes or No
Metabolism	CYP1A2 inhibitor	No	Yes or No
Metabolism	CYP2C19 inhibitor	No	Yes or No
Metabolism	CYP2C9 inhibitor	No	Yes or No
Metabolism	CYP2D6 inhibitor	No	Yes or No
Metabolism	CYP3A4 inhibitor	No	Yes or No
Excretion	Total clearance	-0.953	Log mL min^{-1} kg^{-1}
Excretion	Renal OCT2 substrate	No	Yes or No

be seen from Table 3 that the probability (p) values for all toxic properties are quite low (<1) and predictions results does not predict any toxic effects such as hepatotoxicity (p = 0.99), carcinogenicity (p = 0.88), immune-toxicity (p = 0.99), mutagenicity (0.74), cytotoxicity (p = 0.78) and AMES toxicity (p = 0.91). It is also confirmed from Table 3 that for all these toxicities none of the p values is >1, therefore, HA is non-toxic. However, it should be given to the patient in a small amount as it may cause some allergic reactions. The Pharmacokinetics properties of HA were also determined to check its absorption, distribution, metabolism and excretion rates (Table 3). In Table 3, it was observed that the HA has -3.908 log mol^{-1} solubility in water, which means that it does not dissolve in liquid instead it will reach its target proteins and will bind effectively. The 0% intestinal absorption shows that it will not absorb into the intestine and will reach its target. It was also observed from Table 3 that HA is a non-inhibitor of several enzymes such as, P-glycoprotein I, P-glycoprotein II, CYP1A2, CYP2C19, CYP2C9, CYP2D6, CYP3A4 showing it will not affect the metabolic rate of the individual after administering into the body. Similarly, from distribution a property, it was observed that HA has human unbound fraction 0.675, blood-brain barrier permeability -3.026 and central nervous system permeability -3.824 means it will not cross the blood-brain barrier and central nervous system.

The HA ligand was docked one by one into the mutated pockets of proteins: BMP2, COL1A, IGF-1, PDGF and TGF-β. For determining the finest position of the docked complexes, the docking scores were calculated along with binding positions. The interactive amino acids identified in BMP2: HA docked complex include GLY45, CYS43, HIS44, ARG114 and GLN64. For COL1A: HA were ASP129, SER125, LYS70 and ARG34, similarly,

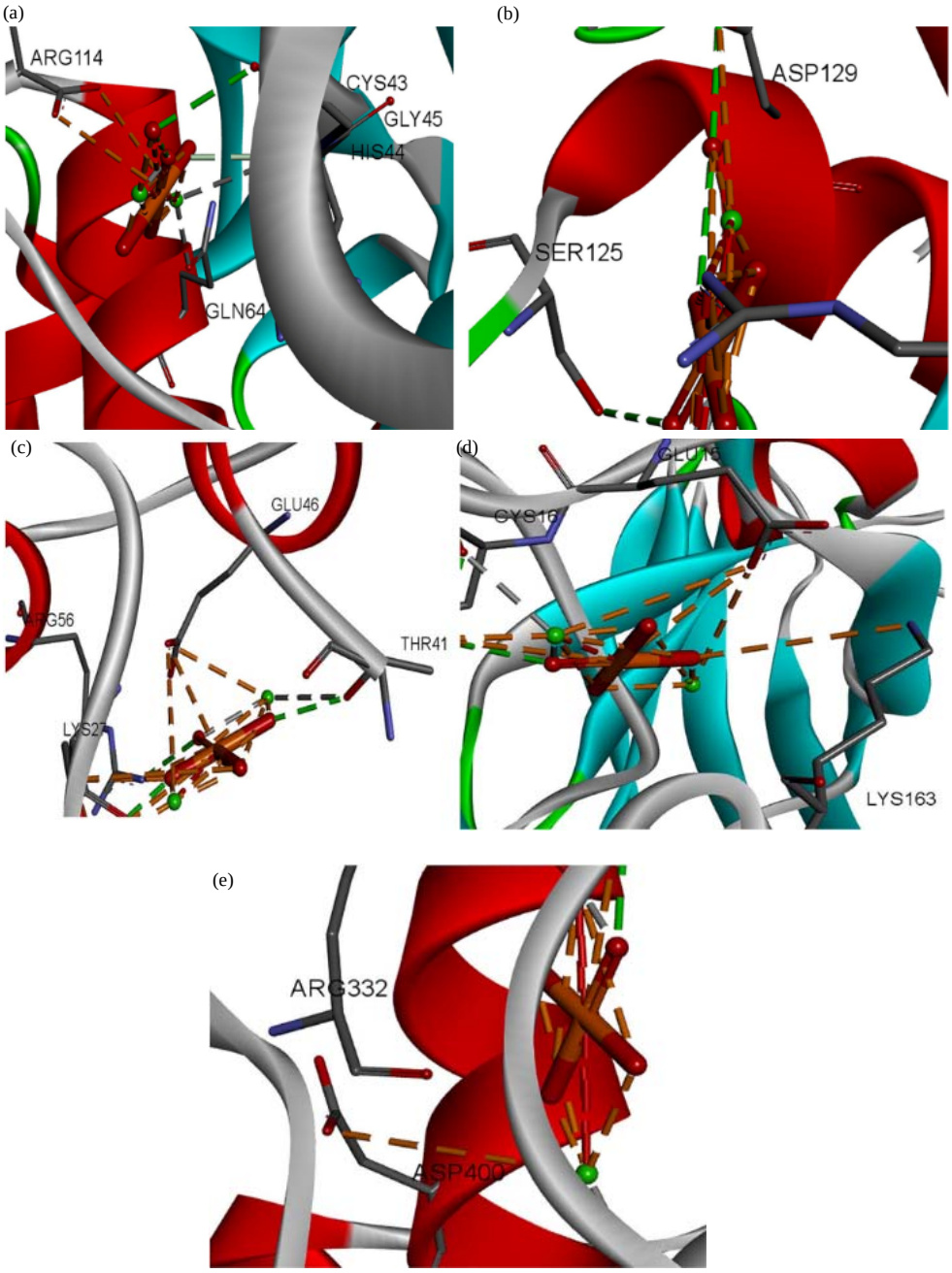

Fig. 3(a-e): Docked complexes of HA ligand with bone healing proteins BMP2, COL1A, IGF-1, PDGF and TGF-β, (a) BMP2: HA complex, (b) COL1A: HA, (c) Docked complex of IGF-1: HA, (d) Molecular docking results of PDGF: HA and (e) TGF-β: HA complex

Red spiral figure shows the alpha helices, whereas blue ribbons represent Beta sheets, the turns and coils in the proteins are shown by gray color

the interacting amino acids in the IGF-1: HA complexes were found to be GLU46, ARG56, THR41 and LYS27. In a docked complex of PDGF: HA the interacting amino acids were CYS16, LU15 and LYS163, for GF-B: HA were TYR378, ARG332 and ASP400. The results of the Docking are shown in Fig. 3-5.

From Fig. 3, it was observed that amino acids of all the active pockets of proteins make several bonds with HA. The interactive amino acids identified in BMP2: HA docked complex in Fig. 3a include GLY45, CYS43, HIS44, ARG114 and GLN64. For COL1A: HA in Fig. 3b were ASP129, SER125, LYS70 and ARG34, similarly, the interacting amino acids in the IGF-1:

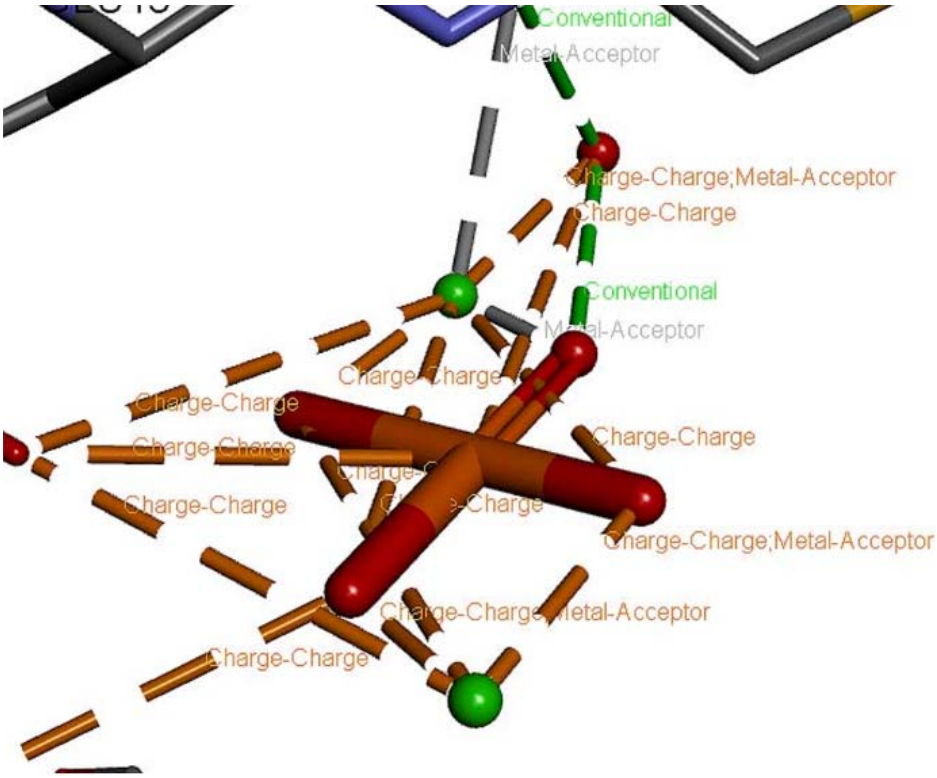

Fig. 4: Type of bonds formed in all the docked

Table 4: Details of docking results of HA with the bone healing proteins

Docked complexes	Binding energy (kcal mol^{-1})	Binding efficiency (kcal mol^{-1})	Torsional energy	Inhibition constant (μM)
BMP2:HA	-11.62	0.896	0.45	2.41
COL1A:HA	-11.36	0.791	0.5	2.01
IGF-1:HA	-9.69	0.881	0.5	2.65
PDGF:HA	-9.59	0.874	0.48	2.21
TGF-β:HA	-7.088	0.873	0.45	2.39

HA complex in Fig. 3c, were found to be GLU46, ARG56, THR41 and LYS27. In a docked complex of PDGF: HA in Fig. 3d the interacting amino acids were CYS16, LU15 and LYS163, for TGF-β: HA in Fig. 3e was TYR378, ARG332 and ASP400. As, HA makes the bond with the maximum number of pocket residues which confirm the efficacy of HA as a strong inhibitor of these mutated genes.

In Fig. 4, the maximum number of Charge-charge and charge-charge; metal acceptor bonds were identified, a few conventional bonds were also observed.

From Fig. 5a-e, it was observed that when the surface analysis was performed for all the docked results, the HA ligand fit effectively under the surface without damaging the surface, representing its stability and appropriate docking. In all the docked complexes, The HA cumulative binding energy, binding efficiency, torsional energy and inhibition constants were calculated in Table 4.

Table 4 shows the docked complexes of HA. In all the docked complexes, BMP2: HA, COL1A: HA, IGF-1:HA, PDGF: HA and TGF-β: HA the binding energies were -11.62, -11.36, -9.69, -9.59 and -7.088 kcal mol^{-1}, BMP2: HA and COL1A: HA respectively shown better binding affinity than other complexes, compounds which have more negative binding energies and higher Binding efficiencies (docking scores) >0.5 indicates the better binding to the desired protein. In all the complexes, the docking scores were also greater than 0.5 and were lying in the range of 0.79-0.89. The HA compound is quite better for binding if the binding energies are in negative values. Similarly, the binding efficiency tells about the docking score. Positive inhibition constant values >2.0 for all the docked complexes in Table 4 showed that the HA ligand is powerful in the binding perspective. Herein, the purpose of molecular docking was to assess the HA interactions with the pocket atoms of selected bone healing genes. Therefore, the

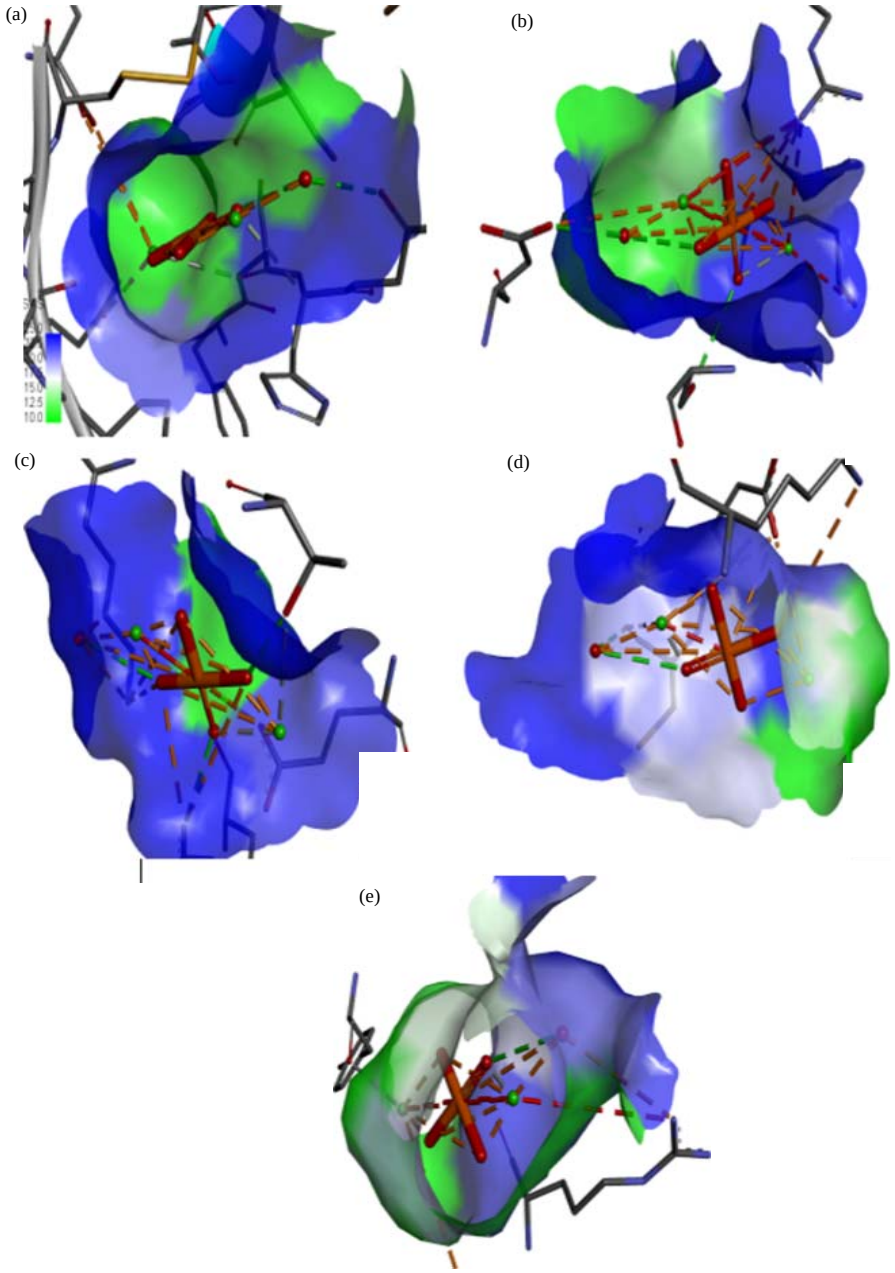

Fig. 5(a-e): Surface analysis of the docked complexes of HA ligand with bone healing proteins, (a) BMP2: HA complex, (b) COL1A: HA, (c) Docked complex of IGF-1: HA, (d) Molecular docking results of PDGF: HA and (e) TGF-β: HA complex

nano-sized HA powder synthesized in this study can also be directly given to patients in the form of capsules to repair the mutated genes. MD experiments were performed on the diverse behaviour of the HA ligand at the active site of proteins, thereby further supporting the molecular docking. For HA ligand with chosen proteins, MD run for 10 ns were initiated with the best dock poses. A total of 5 docked results were subjected to MD simulations and the results were read as RMSD and potential energy profiles. It was determined that the RMSD of all complexes was below 0.4 nm. After observing the RMSD plots, it was discovered that during the initial MD phases, minor variations were noticed; however, all the docked systems seemed to be well converged after 4000 ns, showing no significant variations. These findings, thus, guarantee the stability of the proteins. Also, during the entire simulations, they have shown constant potential energy without any difference and were found to be stable at -kJ mol^{-1} in Fig. 6.

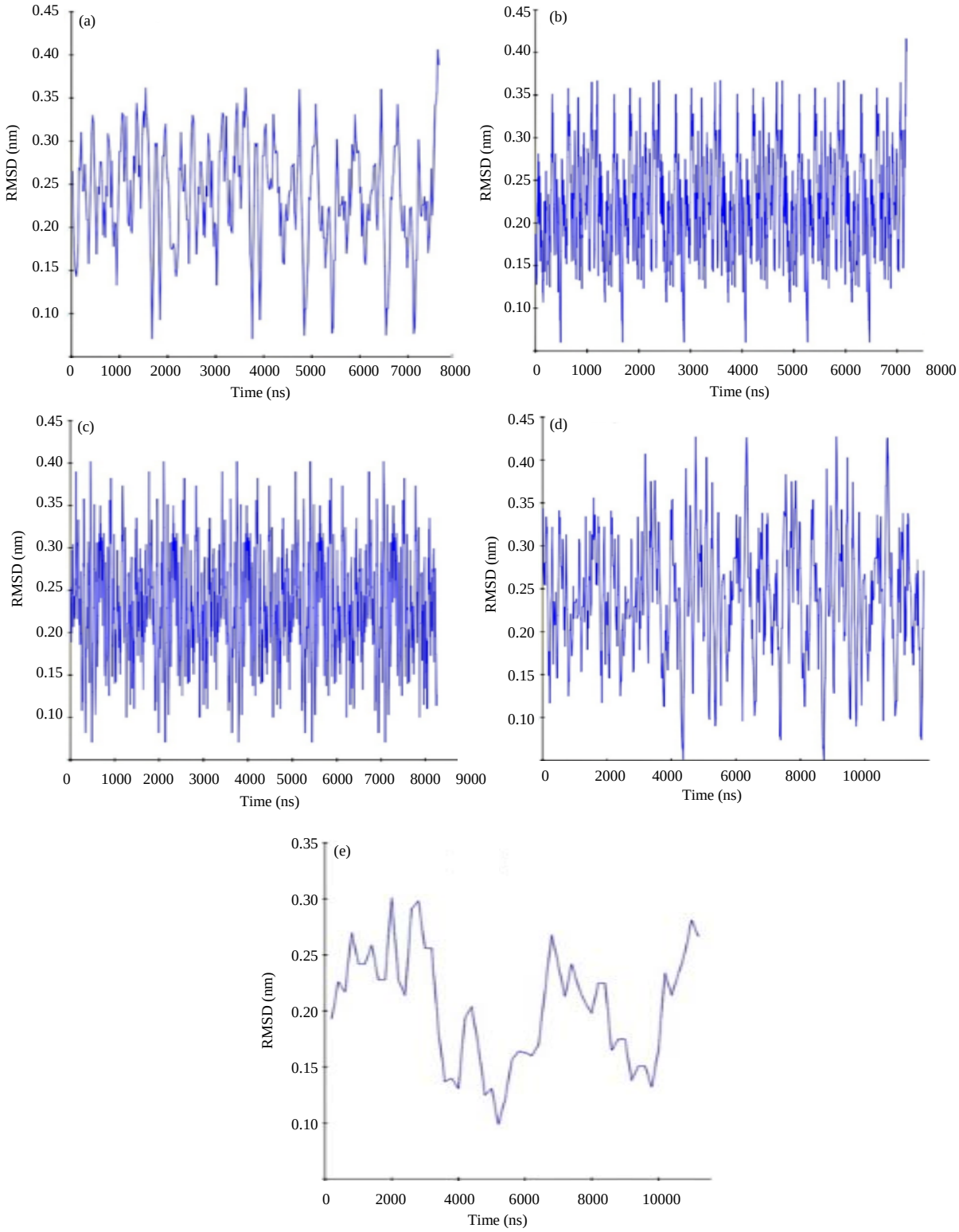

Fig. 6(a-e): Molecular dynamics simulation analysis of the docked complexes of HA ligand with bone healing proteins, (a) BMP2: HA complex, (b) COL1A: HA, (c) Docked complex of IGF-1: HA, (d) TGF-β: HA complex and (e) Molecular docking results of PDGF: HA

Y-axis represents RMSD values in nano-meter (nm) and X-axis shows time in nano seconds (ns)

It was determined from Fig. 6a-e that the RMSD of all complexes was below 0.4 nm. It is observed from Fig. 6a that simulations were performed for 8000 ns and the majority of peaks were lying in the 0.15-0.33 RMSD, in Fig. 6b, MD simulations were performed for 8000 ns and the majority of peaks were observed between 0.13-0.35 RMSD, Fig. 6c shows, similar results as Fig. 6a, the only difference is MD simulations time which is 9000 ns in case of Fig. 6c, Fig. 6d shows MD simulations for 10000 ns and the density of peaks was observed between 0.20-0.33 RMSD, whereas from Fig. 6e, it was observed that during 10000 ns MD simulations diverse nature of peaks were observed lying in the RMSD value of 0.10-0.3. After observing the RMSD plots, it was discovered that during the initial MD phases, minor variations were noticed; however, all the docked systems seemed to be well converged after 4000 ns, showing no significant variations. These findings, thus, guarantee the stability of the proteins. Also, during the entire simulations, they have shown constant potential energy without any difference and were found to be stable at -10 kJ mol^{-1}.

DISCUSSION

Over the last decades, many scientists have been working on HA synthesis for the application of bone tissue obtaining materials of different shapes and proportions. This research, therefore, focuses on the preparation of nano-sized HA in the form of plates or rods, similar to the HA present in human bones. In the biomedical field, nano-sized hydroxyapatite has also gained increasing attention due to its unusual structural properties, such as large surface area and practical nano-sized volume, which are believed to have increased biological activity and the ability to serve as functional nanocarriers for bone-related therapies[30-32]. Wang *et al.*[33] used the zeta potential study to manufacture and analyze nanoparticles. They also utilized surfactants to see the HA growth on the surface of the oyster shell using Fourier transform infrared spectroscopy and X-ray diffraction. The Zeta Potential (ZP) of the produced HA was altered by different surfactants, which exhibited the opposite potential value. However, this study synthesized HA nanorod composite powders using calcium nitrate tetrahydrate and diammonium hydrogen phosphate as precursors at low temperatures and constant pH (10.5). Conventional heated analyses of HA powder at 1000°C did not contain any calcium hydroxide and displayed intertwined porosity that could contribute to osseointegration, local drug delivery and the circulation of physiological fluids contributing to the development of new bones.

Zhang *et al.*[34] created a safe, non-toxic and effective oral insulin delivery system based on hydroxyapatite nanoparticles functionalized with polyethylene glycol that reduced blood glucose levels in type 1 diabetic mice. It can assist gallic acid and insulin in successfully escaping gastrointestinal enzymes and delivering insulin into the systemic circulation, so activating the insulin signalling pathway. Whereas, have synthesized nanosize HA rods to treat several gene mutations responsible for causing bone damage, the nanosize HA in this study acts as a synthetics medicine.

Phatai *et al.*[35] characterized the HA nanoparticles using Fourier transform and X-ray diffractions and obtained the hexagonal framework of HA and rhombohedral structure. However, characterization of produced nano-sized HA powder was also done in this study by creating dense and porous samples. Used the cold pressing method to successfully prepare dense HA powder samples, Sintering at 1250°C resulted in an apparent density of 2.346 g cm^{-3}.

A higher flexural strength (56.9 MPa) was obtained by the mechanical test of the dense samples, thus demonstrating its suitability for load-bearing bone implant applications. Porous bodies were also developed using the sol-gel derived HA powder from sponge impregnation technique, porous samples had an apparent density of 1.180 g cm^{-3}, with a flexural strength of 1.89 MPa, demonstrating that these HA samples can be used to replace human spongy bone. Therefore, the physical characterization of the nano-sized HA powder accompanied by the preliminary powder performance test in the development of porous and dense samples reveals that the powder has excellent physical properties and dense and porous bioactive bone implants with desirable properties can be made.

The toxicity of a substance is determined to establish its side effects and it is an important factor in the advancement of treatments. Mechanism-based toxicity, off-target toxicity, immunological hypersensitivity, bioactivation and, in rare situations, covalent modification are used to define the causes of drug toxicity[31]. Usually, all the compounds produce toxicity at high doses and are safer at exceptionally low doses. Therefore, in this study, the purpose of identifying the toxic effects of HA was to determine its adverse effects, for the case if it is given to the patient in the form of capsules for bone repair. Similarly, the ADME properties of HA were also predicted in this study, because the composition of a substance specifies its physical characteristics, chemical properties, toxicity and ADME. The higher the absorption rate of a compound, it is more likely it to be an effective drug, similarly higher elimination rate makes a drug nontoxic[32].

Molecular docking is a tool developed in the in-silico structure process that is commonly used in drug development. Docking enables the classification of novel therapeutic compounds, the prediction of ligand-target interactions at the molecular level and the delineation of structure-activity correlations (SARs) without prior knowledge of any target modulator's chemical composition[32]. Results of molecular docking also shown that all docked complexes have lower binding energies and better binding scores. All the complexes have demonstrated structural diversity. Inside the active site, the comparatively small HA compound had more freedom to be accommodated and a linear conformation within the protein active sites was adapted. Information on the main residues needed for inhibition was provided by the exploration of molecular interactions. Arginine, Lysine and Tyrosine were found to be common interacting amino acids in all the docked complexes.

CONCLUSION

Using calcium nitrate tetrahydrate and diammonium hydrogen phosphate, hydroxyapatite powders with nanoscale were successfully prepared using co-precipitation. The HA particles have a rod-like structure as analyzed under TEM, with a 100-200 nm average length. The results synthesized nanopowder is in great concurrence with those got by morphological examination. The obtained nanosize HA powder was about 100% pure. In short, the technique of co-precipitation offers a simple and economical route to achieve nanosized HA. Also, the molecular docking studies to determine the effectiveness of HA validated it as an effective binding agent for bone repair. The negative binding energies and positive binding affinity values demonstrate HA as a potent inhibitor of mutated bone healing genes (BMP2, COL1A, IGF-1, PDGF and TGF-β). In the future, this work can be further accessed in clinical trials to determine the efficacy of HA against the above-listed gene mutations.

SIGNIFICANCE STATEMENT

This study discovered HA as synthetic medicine that can be beneficial for repairing bone damage caused by several genes, moreover, this study will help the researchers to uncover the critical areas of pharmaceutical design that many researchers were not able to explore. Thus a new theory on drug design and development may be arrived at.

ACKNOWLEDGMENT

The authors are grateful to Cangzhou Hospital of Integrated Traditional Chinese and Western Medicine of Hebei Province. The final version of the manuscript is approved by all the authors.

REFERENCES

1. Vigni, G.E., G. Sabbioni, A. Tomasi and E. Gervasi, 2020. Nonunion and malunion in proximal humerus fractures. Lo Scalpello, 34: 3-8.
2. Compston, J., A. Cooper, C. Cooper, N. Gittoes and C. Gregson *et al*., 2017. UK clinical guideline for the prevention and treatment of osteoporosis. Arch. Osteoporosis, Vol. 12. 10.1007%2Fs11657-017-0324-5.
3. Loi, F., L.A. Córdova, J. Pajarinen, T.H. Lin, Z. Yao and S.B. Goodman, 2016. Inflammation, fracture and bone repair. Bone, 86: 119-130.
4. Marongiu, G., A. Dolci, M. Verona and A. Capone, 2020. The biology and treatment of acute long-bones diaphyseal fractures: Overview of the current options for bone healing enhancement. Bone Rep., 10.1016/j.bonr.2020.100249.
5. Maridas, D.E., M. Feigenson, N.E. Renthal, S.M. Chim, L.W. Gamer and V. Rosen, 2020. Bone Morphogenetic Proteins. In: Principles of Bone Biology, Bilezikian, J.P., T.J. Martin and C.J. Rosen (Eds.)., Elsevier Inc., pp: 1189-1197.
6. Narasimhulu, C.A. and D.K. Singla, 2020. The role of bone morphogenetic protein 7 (BMP-7) in inflammation in heart diseases. Cells, Vol. 9. 10.3390/cells9020280.
7. Yan, T., J. Li, X. Zhou, Z. Yang and Y. Zhang *et al*., 2020. Genetic determinants of fracture non-union: A systematic review from the literature. Gene, Vol. 751. 10.1016/j.gene.2020.144766.
8. Wei, B., C. Wang, C. Yan, B. Tang and X. Yu *et al*., 2020. Osteoprotegerin/bone morphogenetic protein 2 combining with collagen sponges on tendon-bone healing in rabbits. J. Bone Mineral Metab., 38: 432-441.
9. Chow, W.A., 2018. Chondrosarcoma: Biology, genetics, and epigenetics. F1000Res., Vol. 7. 10.12688/f1000research. 15953.1.
10. Xu, X. and X. Cao, 2020. Transforming Growth Factor-β and Skeletal Homeostasis. In: Principles of Bone Biology, Xu, X. and X. Cao (Eds.)., Elsevier, pp: 1153-1187.
11. Vandenput, L., K. Sjögren, J. Svensson and C. Ohlsson, 2012. The role of IGF-1 for fracture risk in men. Front. Endocrinol., Vol. 3. 10.3389/fendo.2012.00051.
12. Caplan, A.I. and D. Correa, 2011. PDGF in bone formation and regeneration: New insights into a novel mechanism involving MSCs. J. Orthop. Res., 29: 1795-1803.

13. Baht, G.S., P. Nadesan, D. Silkstone and B.A. Alman, 2017. Pharmacologically targeting beta-catenin for NF1 associated deficiencies in fracture repair. Bone, 98: 31-36.
14. Wang, Q., J. Yan, J. Yang and B. Li, 2016. Nanomaterials promise better bone repair. Mater. Today, 19: 451-463.
15. Kolanthai, E., K. Ganesan, M. Epple and S.N. Kalkura, 2016. Synthesis of nanosized hydroxyapatite/agarose powders for bone filler and drug delivery application. Mater. Today Commun., 8: 31-40.
16. Anwar, A., Q. Kanwal, S. Akbar, A. Munawar, A. Durrani and M.H. Farooq, 2017. Synthesis and characterization of pure and nanosized hydroxyapatite bioceramics. Nanotechnol. Rev., 6: 149-157.
17. Johansson, P., R. Jimbo, Y. Kozai, T. Sakurai, P. Kjellin, F. Currie and A. Wennerberg, 2015. Nanosized hydroxyapatite coating on peek implants enhances early bone formation: A histological and three-dimensional investigation in rabbit bone. Materials, 8: 3815-3830.
18. Tram Do, T.N., W.H. Lee, C.Y. Loo, A.V. Zavgorodniy and R. Rohanizadeh, 2012. Hydroxyapatite nanoparticles as vectors for gene delivery. Ther. Delivery, 3: 623-632.
19. Güler, H., G. Gündoğmaz, F. Kurtuluş, G. Çelik and Ş.S. Gacanoğlu, 2011. Solid state synthesis of calcium borohydroxyapatite. Solid State Sci., 13: 1916-1920.
20. Sopyan I., R. Singh and M. Hamdi, 2008. Synthesis of nano sized hydroxyapatite powder using sol-gel technique and its conversion to dense and porous bodies. Indian J. Chem., 47: 1626-1631.
21. Lou, Z., Y. Wang, Y. Yang, Y. Wang and C. Qin *et al*., 2020. Carbon sphere template derived hollow nanostructure for photocatalysis and gas sensing. Nanomaterials, Vol. 10. 10.3390/nano10020378.
22. Wang, Y.J., C. Lai, K. Wei, X. Chen, Y. Ding and Z.L. Wang, 2006. Investigations on the formation mechanism of hydroxyapatite synthesized by the solvothermal method. Nanotechnology, Vol. 17.
23. Yao, H.L., G.C. Ji, Q.Y. Chen, X.B. Bai, Y.L. Zou and H.T. Wang, 2018. Microstructures and properties of warm-sprayed carbonated hydroxyapatite coatings. J. Thermal Spray Technol., 27: 924-937.
24. Oliveira, J.M., S.A. Costa, I.B. Leonor, P.B. Malafaya, J.F. Mano and R.L. Reis, 2009. Novel hydroxyapatite/carboxymethylchitosan composite scaffolds prepared through an innovative "autocatalytic" electroless coprecipitation route. J. Biomed. Mater. Res. Part A, 88A: 470-480.
25. Varma, H.K. and S.S. Babu, 2005. Synthesis of calcium phosphate Bioceramics by citrate gel pyrolysis method. Ceramics Int., 31: 109-114.
26. Banerjee, P., A.O. Eckert, A.K. Schrey and R. Preissner, 2018. ProTox-II: A webserver for the prediction of toxicity of chemicals. Nucleic Acids Res., 46: W257-W263.
27. Burley, S.K., H.M. Berman, G.J. Kleywegt, J.L. Markley, H. Nakamura and S. Velankar, 2017. Protein Data Bank (PDB): The Single Global Macromolecular Structure Archive. In: Protein Crystallography. Methods in Molecular Biology, Wlodawer, A., Z. Dauter and M. Jaskolski (Eds.)., Springer, Cham, New York, ISBN-13: 978-1-4939-6998-2, pp: 627-641.
28. Leelananda, S.P. and S. Lindert, 2016. Computational methods in drug discovery. Beilstein J. Org. Chem., 12: 2694-2718.
29. Molino, G., M.C. Palmieri, G. Montalbano, S. Fiorilli and C. Vitale-Brovarone, 2020. Biomimetic and mesoporous nano-hydroxyapatite for bone tissue application: A short review. Biomed. Mater., Vol. 15. 10.1088/1748-605x/ab5f1a.
30. Guengerich, F.P., 2011. Mechanisms of drug toxicity and relevance to pharmaceutical development. Drug Metab. Pharmacokinet., 26: 3-14.
31. Han, Y., J. Zhang, C.Q. Hu, X. Zhang, B. Ma and P. Zhang, 2019. *In silico* ADME and toxicity prediction of ceftazidime and its impurities. Front. Pharmacol., Vol. 10. 10.3389/fphar. 2019.00434.
32. Pinzi, L. and G. Rastelli, 2019. Molecular docking: Shifting paradigms in drug discovery. Int. J. Mol. Sci., Vol. 20. 10.3390/ijms20184331.
33. Wang, Z., S. Jiang, Y. Zhao and M. Zeng, 2019. Synthesis and characterization of hydroxyapatite nano-rods from oyster shell with exogenous surfactants. Mater. Sci. Eng.: C, Vol. 105. 10.1016/j.msec.2019.110102.
34. Zhang, Y., L. Zhang, Q. Ban, J. Li, C.H. Li and Y.Q. Guan, 2018. Preparation and characterization of hydroxyapatite nanoparticles carrying insulin and gallic acid for insulin oral delivery. Nanomed.: Nanotechnol. Biol. Med., 14: 353-364.
35. Phatai, P., C.M. Futalan, S. Utara, P. Khemthong and S. Kamonwannasit, 2018. Structural characterization of cerium-doped hydroxyapatite nanoparticles synthesized by an ultrasonic-assisted sol-gel technique. Results Phys., 10: 956-963.